SCIENCE CHINA
Earth Sciences

SPECIAL TOPIC: China since the Last Glacial Maximum
•RESEARCH PAPER•

August 2019 Vol.62 No.8: 1241–1255
https://doi.org/10.1007/s11430-018-9266-8

A multi-model analysis of glacier equilibrium line altitudes in western China during the last glacial maximum

Dabang JIANG[1,2,3,4*], Yeyi LIU[1,4] & Xianmei LANG[1,2,3]

[1] *Institute of Atmospheric Physics, Chinese Academy of Sciences, Beijing 100029, China;*
[2] *CAS Center for Excellence in Tibetan Plateau Earth Sciences, Beijing 100101, China;*
[3] *Collaborative Innovation Center on Forecast and Evaluation of Meteorological Disasters, Nanjing University of Information Science & Technology, Nanjing 210044, China;*
[4] *University of Chinese Academy of Sciences, Beijing 100049, China*

Received February 13, 2018; revised August 24, 2018; accepted August 31, 2018; published online October 24, 2018

Abstract Based on numerical experiments undertaken with nine climate models, the glacier equilibrium line altitudes (ELAs) in western China during the last glacial maximum (LGM) are investigated to deepen our understanding of the surface environment on the Tibetan Plateau. Relative to the preindustrial period, the summer surface air temperatures decrease by 4–8°C while the annual precipitation decreases by an average of 25% across the Tibetan Plateau during the LGM. Under the joint effects of reductions in summer temperature and annual precipitation, the LGM ELAs in western China are lowered by magnitudes that vary with regions. The ELAs in the southern margin and northwestern Tibetan Plateau decline by approximately 1100 m; the central hinterland, by 650–800 m; and the eastern part, by 550–800 m, with a downward trend from southwest to northeast. The reduction in ELAs is no more than 650 m in the Tian Shan Mountains within China and approximately 500–600 m in the Qilian Mountains and Altai Mountains. The high-resolution models to reproduce the low values of no more than 500 m in ELA reductions in the central Tibetan Plateau, which are consistent with the proxy records from glacier remains. The accumulation zones of the Tibetan Plateau glaciers are mainly located in the marginal mountains during the LGM and have areas 2–5 times larger than those of the modern glaciers but still do not reach the central part.

Keywords Last glacial maximum, Western China, Equilibrium line altitudes, Glacier, Simulation

Citation: Jiang D, Liu Y, Lang X. 2019. A multi-model analysis of glacier equilibrium line altitudes in western China during the last glacial maximum. Science China Earth Sciences, 62: 1241–1255, https://doi.org/10.1007/s11430-018-9266-8

1. Introduction

Earth's climate has dramatically changed in the past, and the study of this fact and the causes of such changes is of great significance to our knowledge of the Earth's environmental evolution and our understanding of modern climate. The last glacial maximum (LGM, approximately 21000 calendar years before present) was a period of the maximum ice advances in the latest ice age, characterized by large-scale ice sheet expansion and the low-level atmospheric greenhouse gas concentrations (Clark et al., 2009). During this period, approximately 24% of the global continent was covered by ice sheets, including the middle and high latitudes in North America, northwestern Europe, and Antarctica, while the counterpart is only 11% at present (Wang and Wen, 2011). Glaciers and permafrost were also widely developed during the LGM (Saito et al., 2013; Liu and Jiang, 2016), and sea level was approximately 130 m lower than at present due to the formation of ice sheets (Wang and Wen, 2011). The LGM is distinguished from the present in climate, environment, topography, land-sea distribution, ecosystems, and many other aspects (Clark et al., 2009) and is a key period for

* Corresponding author (email: jiangdb@mail.iap.ac.cn)

investigating the Quaternary glacial climate.

Previous LGM climate reconstructions across China mainly focused on changes in the hydrothermal conditions and monsoons, with less attention to processes in the cryosphere. Note that the Tibetan Plateau and the high-elevation mountains at its periphery contain the largest modern glaciers worldwide, except for the two poles, and there is controversy about the existence of massive glaciers on the Tibetan Plateau during the LGM (Kuhle, 1995; Shi et al., 1997, 2000, 2006; Liu et al., 1999; Shi, 2002b; Su et al., 2014). According to the records of glacier vestiges and landforms on the Tibetan Plateau, the LGM area of glaciers has been estimated as 35×10^4 km^2, equivalent to 7 times the present area, and all of them were scattered mountain glaciers. Relative to the present, it is suggested that the LGM glacier equilibrium line altitudes (ELAs) on the Tibetan Plateau were lowered by 800 m at the eastern part and the southern margin, by 1000–1200 m at the western margin, and by only 300–500 m in the central-western parts, with the last being rare in global mountain glaciers (Shi et al., 1997). Although ice caps existed in some regions, they were insufficient to form ice sheets covering the entire plateau (Shi et al., 1997; Shi, 2002b; Su et al., 2014). Liu et al. (1999, 2002) reviewed pertinent geological records and suggested the presence of massive ice coverage and even ice sheets on the Tibetan Plateau, given an early estimate of 5–9°C cooling during the LGM. Considering that the magnitude of global cooling during the LGM has been re-estimated as twice (9–11°C) the earlier level, the global mean ELAs were proposed to decrease by 1000–1200 m according to a lapse rate of 0.7°C 100 m^{-1}. Altogether, the LGM ELAs on the Tibetan Plateau are critical to our understanding of the local surface environmental changes at this time.

The ELA is a key measure of the mass balance of a glacier and refers to an average elevation where annual accumulation equals annual ablation. Above this elevation is the net accumulation zone, and below is the net ablation zone. Thus, the ELA represents the lowest elevation for potential glacier formation. The ELA variations are mainly affected by local surface air temperatures and precipitation. In particular, temperature determines ice formation and melting, while precipitation determines mass accumulation of the glaciers. Shi et al. (2000) indirectly calculated the mean temperature from June to August (T_{6-8}, °C) and the annual precipitation (P_a, mm) at the ELAs on 16 glaciers in western China and the Batura Glacier in Pakistan and further proposed a statistical relationship between these variables as follows.

$$T_{6-8} = -15.4 + 2.48 \cdot \ln(P_a). \quad (1)$$

The correlation coefficient is 0.94, which is statistically significant at the 90% confidence level. Based on this formula, Zhao et al. (2003) applied the simulated temperature and precipitation from an atmospheric general circulation model (CCM3) to indicate that the LGM ELAs on the Tibetan Plateau were lowered by 300–900 m relative to the modern level, along with a remarkable expansion of glaciers to form an entire ice sheet. Compared with Liu et al. (1999), Zhao et al. (2003) further considered the influence of the precipitation deficit during the LGM on glacier formation, and thus, the ELA decline in their study is relatively smaller. Of importance is that both studies agree with the LGM presence of ice sheets on the Tibetan Plateau. Note that CCM3 is an early version of the atmospheric general circulation model developed by the American National Center for Atmospheric Research, the sea surface temperatures in which are prescribed, and this model lacks descriptions of oceanic dynamics and air-sea interactions. Further, its horizontal resolution of 2.8°×2.8° is too sparse to reflect topographic features. Thus, there is uncertainty in CCM3 simulations of the Tibetan Plateau climate and, in turn, glaciers. In particular, it is failed to reproduce the modern geographical distribution of glaciers and their changes during the LGM over the marginal regions of the Tibetan Plateau on the basis of CCM3 experiments (Zhao et al., 2003).

Based on these premises, this study uses numerical experiments undertaken with nine state-of-the-art climate models participating in the Coupled Model Intercomparison Project Phase 5 (CMIP5), including fully coupled atmosphere-ocean and atmosphere-ocean-vegetation general circulation models, to investigate changes in the ELAs and glacier extents in the mountainous regions of western China (23°–50°N, 70°–105°E) during the LGM, along with the possible underlying mechanisms. Such a multi-model analysis of paleoclimate simulations is expected to advance our understanding of the climate and environmental changes over China during this period.

2. Data and methods

Data applied here are derived from the LGM and preindustrial (reference period) experiments with the nine CMIP5 models, including the surface air temperature at 2 m, precipitation, and the topographic height provided by the models. Basic information about the nine models and their experiments is listed in Table 1, while the coordinated boundary conditions for the LGM and preindustrial experiments are provided in Table 2. Compared with the reference period, the LGM boundary conditions show predominant changes manifested in the land ice sheets and atmospheric concentrations of CO_2, CH_4, and N_2O. More detailed information about the climate models, experimental design, and boundary conditions can be found at the CMIP5 website (https://cmip.llnl.gov/) and in Taylor et al. (2012).

Table 1 Basic information about the nine climate models and their numerical simulations

Model name	Country	Atmospheric horizontal resolution (longitude×latitude) and vertical levels	Integral length (year)
CCSM4	USA	1.25°×~0.9°, L26	100
CNRM-CM5	France	~1.4°×~1.4°, L31	200
COSMOS-ASO	Germany	3.75°×~3.75°, L19	600
FGOALS-g2	China	~2.8°×3°, L26	100
GISS-E2-R	USA	2.5°×2°, L40	100
IPSL-CM5A-LR	France	3.75°×~1.9°, L39	200
MIROC-ESM	Japan	~2.8°×~2.8°, L80	100
MPI-ESM-P	Germany	1.875°×~1. 875°, L47	100
MRI-CGCM3	Japan	1.125°×1.125°, L48	100

Table 2 Comparison between boundary conditions for the LGM and preindustrial (reference period) experiments[a)]

Boundary conditions	Reference period	LGM
Earth's orbital parameters	Eccentricity=0.016724 Obliquity=23.446° Precession=102.04°	Eccentricity=0.018994 Obliquity=22.949° Precession=114.42°
Greenhouse gas concentrations	CO_2=280 ppm CH_4=760 ppb N_2O=270 ppb	CO_2=185 ppm CH_4=350 ppb N_2O=200 ppb
Ice sheets	Modern	Reconstructions

a) 1 ppm=1mg L^{-1}; 1 ppb=1μg L^{-1}

2.1 Model evaluation

The ability of models to reproduce the geographical distribution and amplitude of the modern annual and seasonal temperatures and precipitation across China determines their reliability in simulating the past ELAs to some extent. Before calculating the ELA, we compare the simulated temperature and precipitation in individual preindustrial experiments to the modern observational counterparts, aiming to evaluate the model performance in simulating the climate of western China. The observations are the monthly temperature and precipitation provided by the National Climate Center of the China Meteorological Administration for the period 1970–1999 with a horizontal resolution of 0.5°×0.5°, which were gathered from the 2416 meteorological stations across China (Wu and Gao, 2013). Given that the horizontal resolutions of models range from approximately 1°×1° to 3.75°×3.75° and that the spatial scale of glaciers is relatively small, we remap all the model data into a grid mesh of the observations (0.5°×0.5°) using bilinear interpolation. The spatial correlation coefficients between models and observations and their centered root-mean-square deviations of variables over western China are then calculated.

As shown in Table 3, the correlation coefficients of simulated summer temperatures with observations are 0.90–0.98 for individual models and 0.97 for their multi-model mean (MMM), all significant at the 95% confidence level. The centered root-mean-square deviation lies within the range of 2.71–4.84°C for individual models and is 2.82°C for the MMM. These results suggest that all the models simulate the geographical distribution and magnitude of summer temperatures in western China reasonably well. The correlation coefficient of annual precipitation ranges from 0.22 to 0.65 among models and is 0.49 for the MMM, and all pass the significance test at the 95% confidence level. The centered root-mean-square deviation is smaller than 4 mm d^{-1} for most models and is 3.47 mm d^{-1} for the MMM, indicating the ability of the models to reasonably reproduce the overall characteristics of annual precipitation across western China. Taken together, the climate models applied here are capable of simulating the climatological state of the modern summer temperatures and annual precipitation over western China, with a better performance on the temperature. The MMM performs better than the majority of individual models.

2.2 ELA calculation

Many methods have been used to calculate the ELA, including statistical models and physical models. For instance, the currently widely used mass-balance and ice-flow model simulates not only the ice volume but also the ELA and temperature and precipitation at this elevation (Xu et al., 2013). The approach based on the mass and energy balance has also been well developed in recent decade, which determines the ELA according to the local climate conditions

Table 3 Statistical relationship of the simulated summer surface air temperature and annual precipitation in western China to the observations for the period 1970–1999[a)]

Models	Spatial correlation coefficient		Centered root-mean-square deviations	
	Summer temperature	Annual precipitation	Summer temperature (°C)	Annual precipitation (mm d^{-1})
CCSM4	0.98	0.47	2.71	3.52
CNRM-CM5	0.96	0.59	3.36	2.97
COSMOS-ASO	0.90	0.48	3.85	4.88
FGOALS-g2	0.97	0.40	3.11	2.56
GISS-E2-R	0.97	0.41	3.01	7.02
IPSL-CM5A-LR	0.97	0.49	3.01	2.75
MIROC-ESM	0.96	0.22	4.84	4.90
MPI-ESM-P	0.98	0.33	2.73	6.09
MRI-CGCM3	0.98	0.65	2.71	2.13
Ensemble	0.97	0.49	2.82	3.47

a) All the spatial correlations are significant at the 95% confidence level. Wu and Gao (2013)

and provides the causes of the ELA changes with direct and explicit physical implications (Rupper and Roe, 2008; Bravo et al., 2015; Duan et al., 2017). However, considering the complexity of these physical models and the multiple variables as input, we use the empirical relationship between summer temperature and annual precipitation at the ELA proposed by Shi et al. (2000) to calculate the ELAs in western China, which is consistent with the study of Zhao et al. (2003). According to eq. (1), only the summer temperature and annual precipitation at the ELA are required for the calculation. We assume the air temperature decreases with elevation at a rate of 0.65°C 100 m^{-1} (for dry atmosphere); thus, the air temperature at the ELA can be estimated by the given temperature at the model topographic height (T_0) and the difference between this height and the ELA (h, units: 100 m) as follows:

$$T_{\mathrm{ELA}} = T_0 - (\Delta T \cdot h). \quad (2)$$

Given that the relationship between precipitation and elevation is complicated and there are sparse meteorological stations across the high-elevation regions, the annual precipitation at the ELA is usually replaced by the mean precipitation at the 2000 m above surface (Shi et al., 1989). Recently, some researchers have used the precipitation recorded by the stations near glaciers as the values at the ELA (Ono et al., 2004; Hebenstreit, 2006; Zhang et al., 2009). To obtain the values closest to the real conditions, we directly take the precipitation at the model topographic height (P_0) as the value at the ELA, shown as follows:

$$P_{\mathrm{ELA}} = P_0. \quad (3)$$

Both T_{ELA} and P_{ELA} in eqs. (2) and (3) are functions of height (h). Substituting them into eq. (1) yields:

$$T_0 - (\Delta T \cdot h) = -15.4 + 2.48 \cdot \ln(P_0). \quad (4)$$

After solving eq. (4) to obtain the single unknown variable h, the ELA can be written as:

$$\begin{aligned}\mathrm{ELA\ (or\ AIG)} &= \mathrm{model\ topographic\ height} + h \cdot 100 \\ &= \mathrm{model\ topographic\ height} \\ &\quad + \left(\frac{T_0 + 15.4 - 2.48 \cdot \ln(P_0)}{\Delta T}\right) \cdot 100. \end{aligned} \quad (5)$$

For each grid point, the ELA can be obtained as long as the summer temperature and annual precipitation are available.

Note that the ELA calculated from eq. (5) is a theoretical value (Lie et al., 2003), representing the minimum elevation of areas climatically suited for glacier formation, and is termed the altitude of instantaneous glacierization (AIG). In reality, glacier formation is determined by not only the climatically constrained AIG but also the topography (Figure 1). To obtain the glacier extent, we compare the AIG calculated from eq. (5) to the real topographic elevation as taken from CRU at a horizontal resolution of 0.5°×0.5° (http://www.cru.uea.ac.uk/) and select regions with topographic elevation higher than the AIG, corresponding to glacier mass net accumulation zones (hereinafter refer to as the accumulation zones) and the potential glacier extents. The relationship of terrain to the ELA and accumulation zones determined by both the summer temperature and annual precipitation is illustrated in Figure 1. Based on the above method, we calculate the ELAs and accumulation zones during the LGM and preindustrial periods, using the summer temperature and annual precipitation simulated by each model, and further obtain the differences between these two periods.

3. Results

3.1 LGM surface air temperature and precipitation changes

Relative to the preindustrial period, the nine models consistently demonstrate that the temperature and precipitation

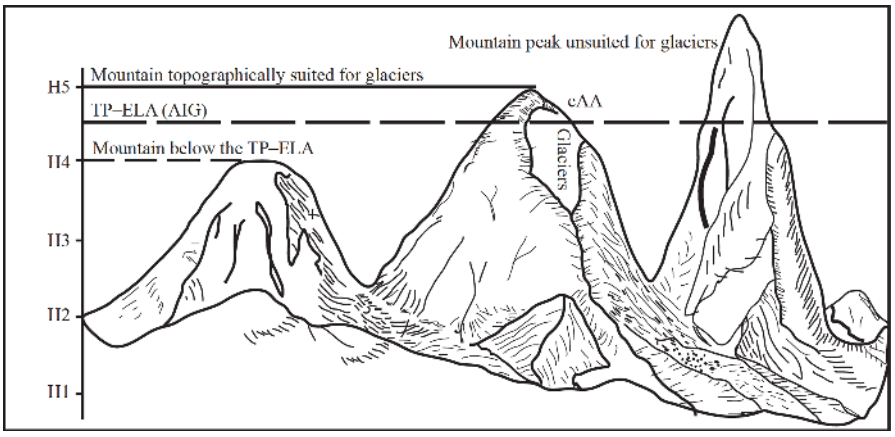

Figure 1 Schematic diagram of the relationship among terrain, the ELA determined by surface air temperature and precipitation (TP-ELA), and climatic accumulation areas (cAA). Adapted from Su et al. (2014).

across western China decreased during the LGM, although the magnitudes of changes vary with models (Figure 2). For the arithmetic multi-model mean (Figures 3 and 4), the seasonal and annual temperatures decrease by 3.95–5.68°C and by 4.80°C, respectively, and the seasonal and annual precipitation decreases by 20–26% and 25%, respectively.

Since the precipitation over most of the glaciers in western China is received in summer, ice ablation and accumulation occur simultaneously during this season (Shi et al., 2000). It is necessary to analyze the summer temperature and precipitation changes. Figure 3c shows that the maximum summer cooling of 5–8°C appears at the periphery of the Tibetan Plateau, and the minimum of only 4–5°C lies in the central plateau. The regions with the greatest cooling resemble those with the largest deficits in precipitation. As mentioned above, the LGM boundary conditions featuring the low-level atmospheric CO_2 concentration and high-latitude ice sheet expansion lead to the large-scale remarkable cooling. For instance, previous sensitivity experiments undertaken by the atmospheric general circulation model indicate that the decrease in atmospheric CO_2 concentration, the cooling of the ocean surface, and the growth of high-latitude ice sheets all gave rise to the temperature decrease in western China. The maximum cooling caused by the above three factors are respectively 0.8, 2.0, and 0.9°C (Jiang and Liang, 2008).

Summer precipitation decreases by 5–10 mm d^{-1} at the southern and western margins of the Tibetan Plateau, which is approximately 10 times the deficit in the central part. Actually, because the climatological mean precipitation at the southern and western margins is an order of magnitude larger than that in the center, the relative reduction in precipitation measured by percentage is smaller at the southern and western margins. Although the absolute reduction in the central-northern part is not large, the corresponding percentage is higher than those in the southern and western margins (Figure 4c). Generally, the percentage of precipitation reduction tends to increase from the southwest margin to the northwest across the plateau. The annual precipitation anomalies are similar to those of summer in the geographical distribution but have smaller magnitudes (Figure 4a). Relative to the preindustrial period, the LGM annual precipitation over western China is decreased by 8–34% among models (Figure 2b).

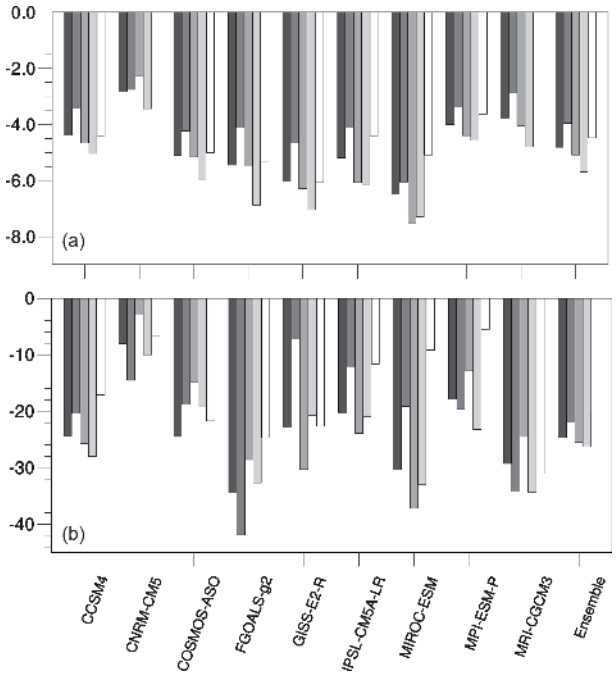

Figure 2 Changes in the LGM annual and seasonal temperature and precipitation in western China relative to the reference period for the individual models and their ensemble mean. (a) Surface air temperature anomalies (°C) and (b) percentage changes in precipitation (%). Bar colors from left dark to right light indicate annual mean, spring, summer, autumn, and winter, respectively.

The causes for the summer precipitation deficit over Eurasia during the LGM have been extensively investigated by previous studies (e.g., Jiang et al., 2015; Tian and Jiang, 2016; Yan et al., 2016). Here, we only briefly review the

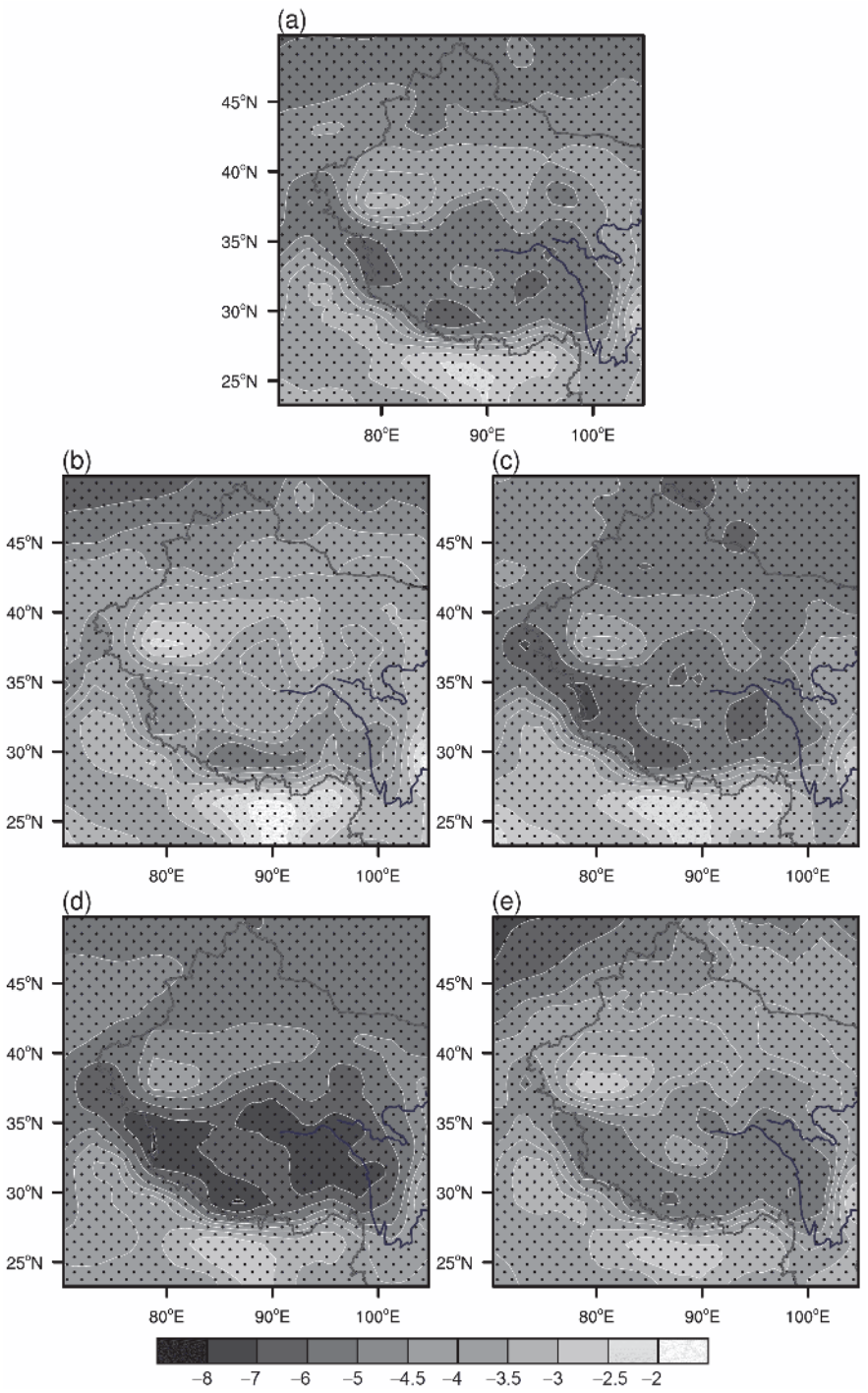

Figure 3 Geographical distribution of the LGM annual and seasonal temperature anomalies relative to the reference period for the multi-model mean (°C). (a) Annual mean, (b) spring, (c) summer, (d) autumn, and (e) winter, with regionally averaged anomalies over western China being −4.80, −3.95, −5.09, −5.68, and −4.46°C, respectively. The dotted areas are significant at the 95% confidence level.

related mechanisms. The analysis of the summer water vapor flux changes during the LGM indicates that the anomalous water vapor flux divergence over western China was associated with the remarkably weakened South and East Asian monsoon circulations, while the reduced water vapor transport in the middle and high latitudes was associated with the weakened zonal winds (Jiang and Tian, 2017). The multi-model studies suggest that in addition to the constraints from changes in the ice sheets and atmospheric greenhouse gas concentrations, the cooling of the ocean surface during the LGM further suppressed the precipitation over western China (Ueda et al., 2011; Tian and Jiang, 2015).

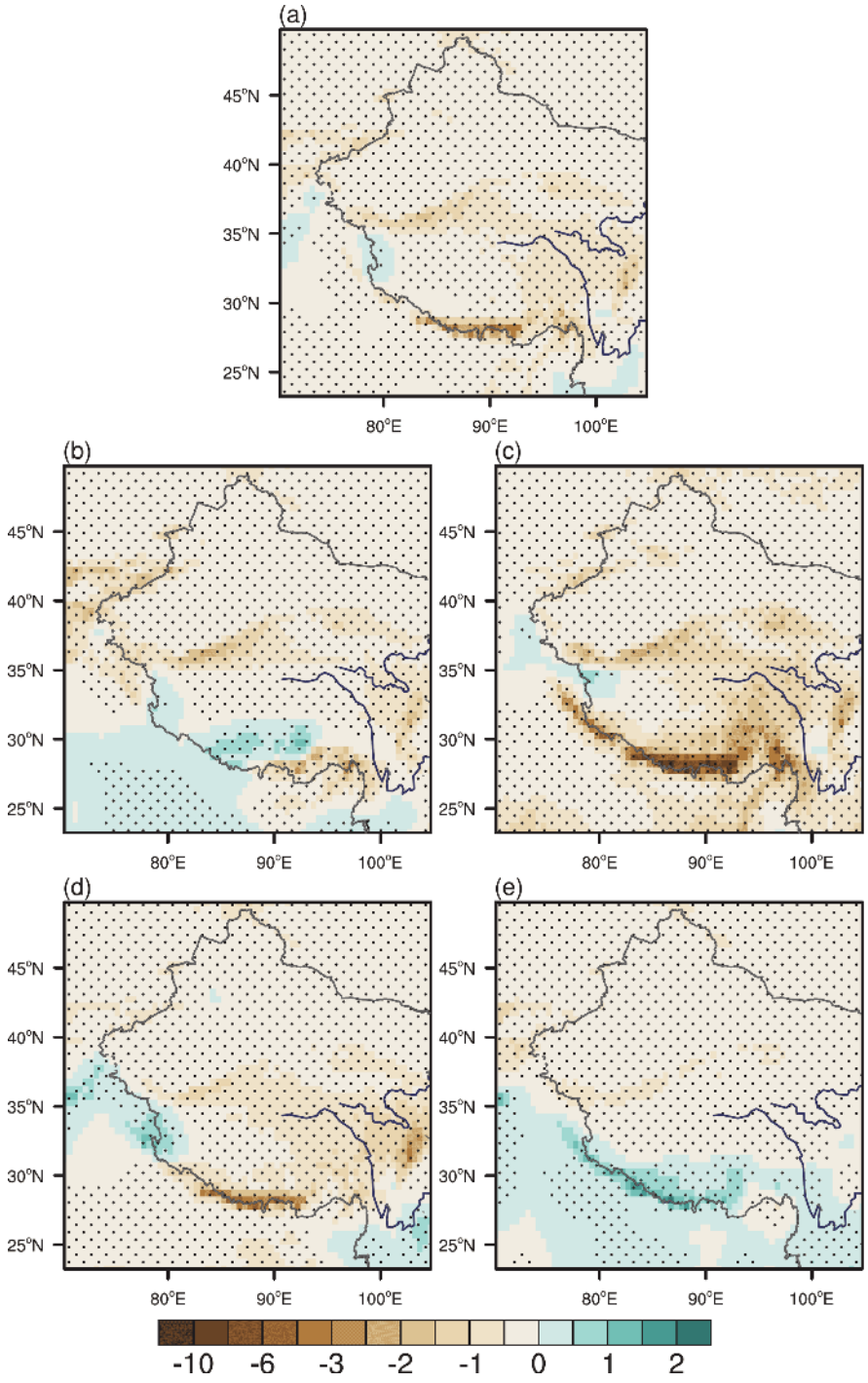

Figure 4 Geographical distribution of the LGM annual and seasonal precipitation anomalies relative to the reference period for the multi-model mean (mm d^{-1}). (a) Annual mean, (b) spring, (c) summer, (d) autumn, and (e) winter, with regionally averaged anomalies over western China being −0.23, −0.22, −0.40, −0.23, and −0.09 mm d^{-1}, respectively. The dotted areas are significant at the 95% confidence level.

3.2 Modern ELA

As shown in Figure 5, the preindustrial ELAs exhibit band-like patterns in most models, consistent with the ELA distributions drawn by Shi et al. (1997, 2000) on the basis of glacier cataloging. The ELAs gradually increase from the marginal mountains to the central Tibetan Plateau, and the contours feature asymmetric zonal patterns with lower values in the southeast and higher values in the northwest. The ELA gradient is large from the eastern and southern margins to the center of the plateau, with a magnitude of approximately 1000 m per degree of latitude, while the gradient decreases to 200–400 m per degree of latitude at the northern margins. The ELA contours over the Tian Shan and Altai

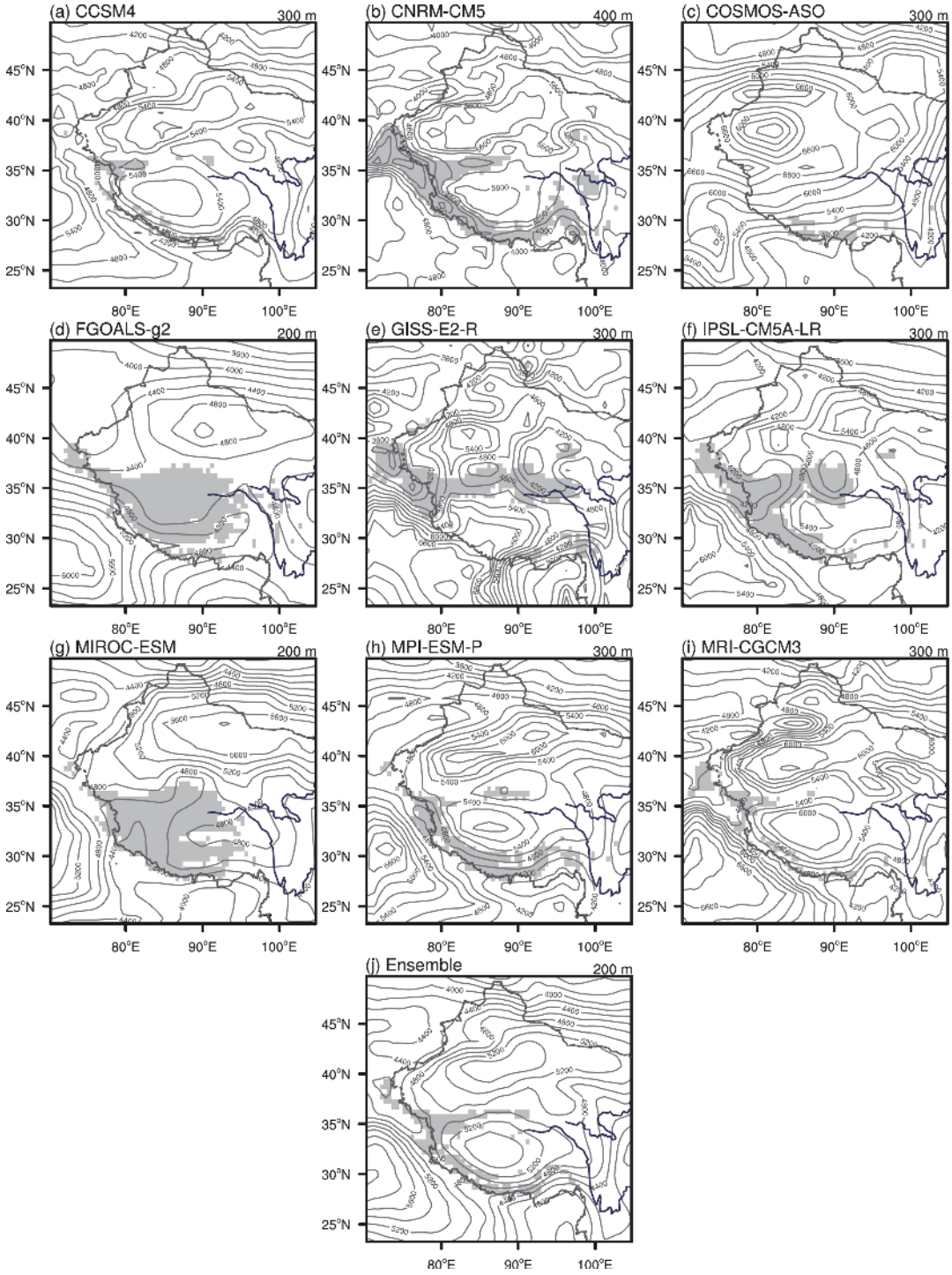

Figure 5 The preindustrial ELA contours determined by the summer temperature and annual precipitation for individual models and their ensemble mean (m). Gray and white indicate the accumulation and non-accumulation zones, respectively. The values at the upper right indicate the contour intervals.

Mountains also feature band-like distributions parallel to each other in the meridional direction.

The distributions and values of the ELA contours vary with models. The high-resolution (low-resolution) models tend to simulate the relatively high (low) ELAs and have a good (poor) inter-model agreement. For example, the four models CCSM4, CNRM-CM5, MPI-ESM-P, and MRI-CGCM3 with horizontal resolutions finer than 2°×2° all simulate the band-like ELA contours of 4200–6000 m across the Tibetan Plateau. The area circled by the 5400 m contour line is large and inclined to the western part of the plateau (Figure 5a, b, h and i). The other five low-resolution models simulate different ELA distributions and values across the Tibetan Plateau. The band-like pattern is not obvious in these models,

and the maximum ELAs in the central plateau range from 4800 to 6000 m. Overall, the ELAs in the low-resolution models are lower than those in the high-resolution models by approximately 300 m, and the accumulation zones are accordingly larger in the low-resolution models.

The MMM results show that ELAs across the Tibetan Plateau lie within 4400–5500 m (Figure 5j), while the ELAs in the Tian Shan and Altai Mountains are 4400–5000 and 3500–3800 m, respectively. The marginal mountains around the Tibetan Plateau constitute accumulation zones, the area of which is small, while most of the central plateau is a non-accumulation zone.

3.3 LGM ELAs

The LGM ELAs are similar to those during the reference period in distributions but have smaller values due to the drier and colder climate, and the accumulation zones expand accordingly (Figure 6). The differences in ELAs of the accumulation zones between the LGM and reference period are shown in Figure 7. In the common accumulation zones for both periods, the MMM indicates that the LGM ELAs are lowered by 393–1440 m, and the LGM accumulation zones expand to 2–5 times larger than the modern extent. For individual models, there is considerable uncertainty regarding the existence of accumulation zones in the central plateau (Figure 7).

The MMM ELAs are 3800–4800 m on the Tibetan Plateau, 3800–4600 m in the Tian Shan Mountains, 2600–3200 m in the Altai Mountains, and approximately 4200 m in the Qilian Mountains during the LGM (Figure 6j). Relative to the reference period, the changes in the LGM ELAs are uneven in western China. The reduction is the largest in the southern margins and the northwestern part of the Tibetan Plateau, especially in the northwestern Himalayas and Karakoram Mountains with decreases of approximately 1100 m, followed by the central part with decreases of 650–800 m, and the reduction is the smallest in the eastern margins with a decrease of approximately 550 m. The lowering of ELAs averages 866 m on the Tibetan Plateau. In response to the ELA changes, the accumulation zones expand into the hinterland of the Tibetan Plateau (Figure 7j). Additionally, ELAs decrease by no more than 650 m in the Tian Shan Mountains within China and by 500–600 m in the Qilian and Altai Mountains.

Note that the four high-resolution models simulate consistent results for the LGM ELA reductions, which are smaller than the results from the other five low-resolution models and the MMM. The reduction obtained from these models lies within 500 m over most of the accumulation zones and is no more than 600 m in the Tian Shan, Altai, and Qilian Mountains; although the accumulation zones expand toward the central Tibetan Plateau, their extents are still limited to the marginal regions and do not reach the hinterland (Figure 7a, b, h, and i).

4. Discussion

4.1 Model ability in simulating ELA

CMIP5 models are able to reasonably reproduce the modern glacier extents and the ELA distributions in western China, especially the high-resolution models. Taking CCSM4 and MRI-CGCM3 as examples, ELA contours over the Tibetan Plateau range from 4200–6000 m during the reference period, and large areas are circled by the 5400 m contour lines; the accumulation zones are scattered throughout the northern Kunlun Mountains, Himalayas, Gangdise Mountains, and central-western Nyainqentanglha Mountains (Figure 5a and i). These characteristics are also seen in the modern ELAs and glacier distributions drawn by Shi et al. (2000) on the basis of glacier cataloging.

Quantitatively, the MMM underestimates the modern ELA values across the Tibetan Plateau, which is derived from cooling biases and excessive precipitation in the CMIP5 models. Relative to observations, the simulated summer temperature over the Tibetan Plateau is colder by 1.8°C on average, and the annual precipitation is overestimated by 1.3 mm d^{-1} (Hu et al., 2014). According to eq. (5), the cooling of summer temperature by 1°C and the excess in annual precipitation of 50–100% can give rise to ELA decreases of 150 m and 150–260 m, respectively. Considering the inherent consistency and coordination of physical processes in climate models, the underestimation of ELAs should also exist in the LGM experiments. The subtraction between the LGM and reference period could largely minimize the above bias, and thus, changes in the ELAs in these two periods are not significantly affected.

The simulated changes in the amplitude and geographical distribution of ELAs during the LGM generally agree with the records from paleo-glacier remains. The maximum lowering of the LGM ELA is approximately 1100 m for the MMM and occurs in the northwestern Tibetan Plateau and the southern margins of the Himalayas. The reduction in ELAs is only 650–800 m in the central plateau and is 550–800 m for the eastern part with a gradual downward trend from the southwest to the northeast (Figure 7j). Except for the central plateau, these simulated changes in ELAs are compatible with the results from Shi et al. (1997). The simulated LGM ELAs in the Qilian, Tian Shan, and Altai Mountains within China decline by approximately 600 m, similar to the values estimated by Shi et al. (1997, 2000) and Shi (2002a). In addition, based on the synthesis of ^{10}Be exposure ages from 1855 individual samples across the Tibetan Plateau and the surrounding mountains, Heyman (2014) suggested that the local ELAs decline by 337±197 m during

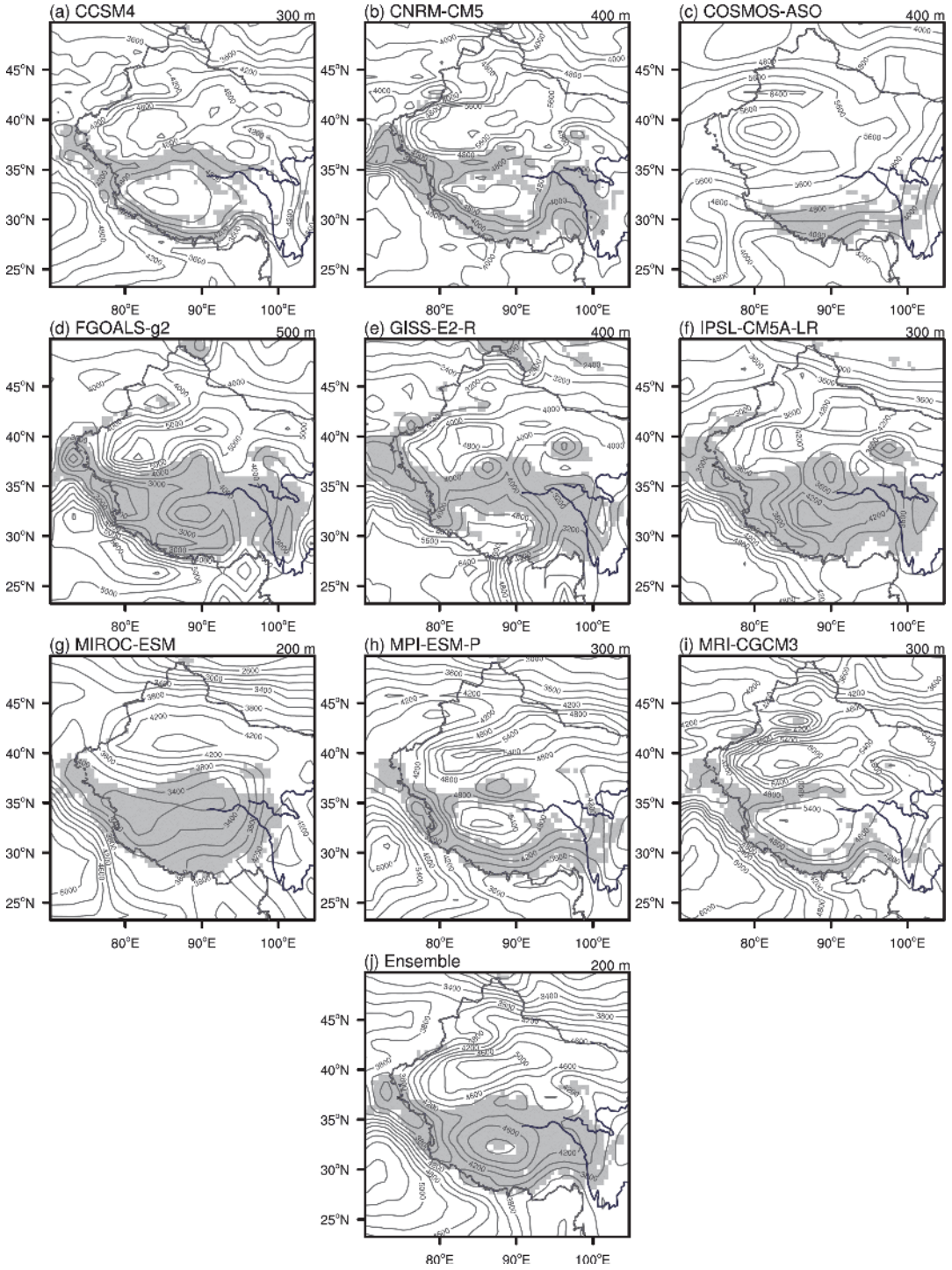

Figure 6 The LGM ELA contours determined by the summer temperature and annual precipitation for individual models and their ensemble mean (m). Gray and white indicate the accumulation and non-accumulation zones, respectively. The values at the upper right indicate the contour intervals.

the LGM, which is also consistent with the model levels. It should be pointed out that the failure of some models to properly simulate the modern existence of accumulation zones in the Tian Shan and Qilian Mountains may be related to the limited horizontal resolution and hence smooth terrain in those models.

We also compare the simulations with the reconstructions from single site records. At a site located in the eastern Himalayas, the ELAs are indicated to have declined by approximately 690 m during the LGM in association with a substantial decrease in temperature (Hu et al., 2017), which is equivalent to the results from the simulations. The glacier records from the western Nyainqentanglha Mountains in the southern Tibetan Plateau suggest that the ELAs descended

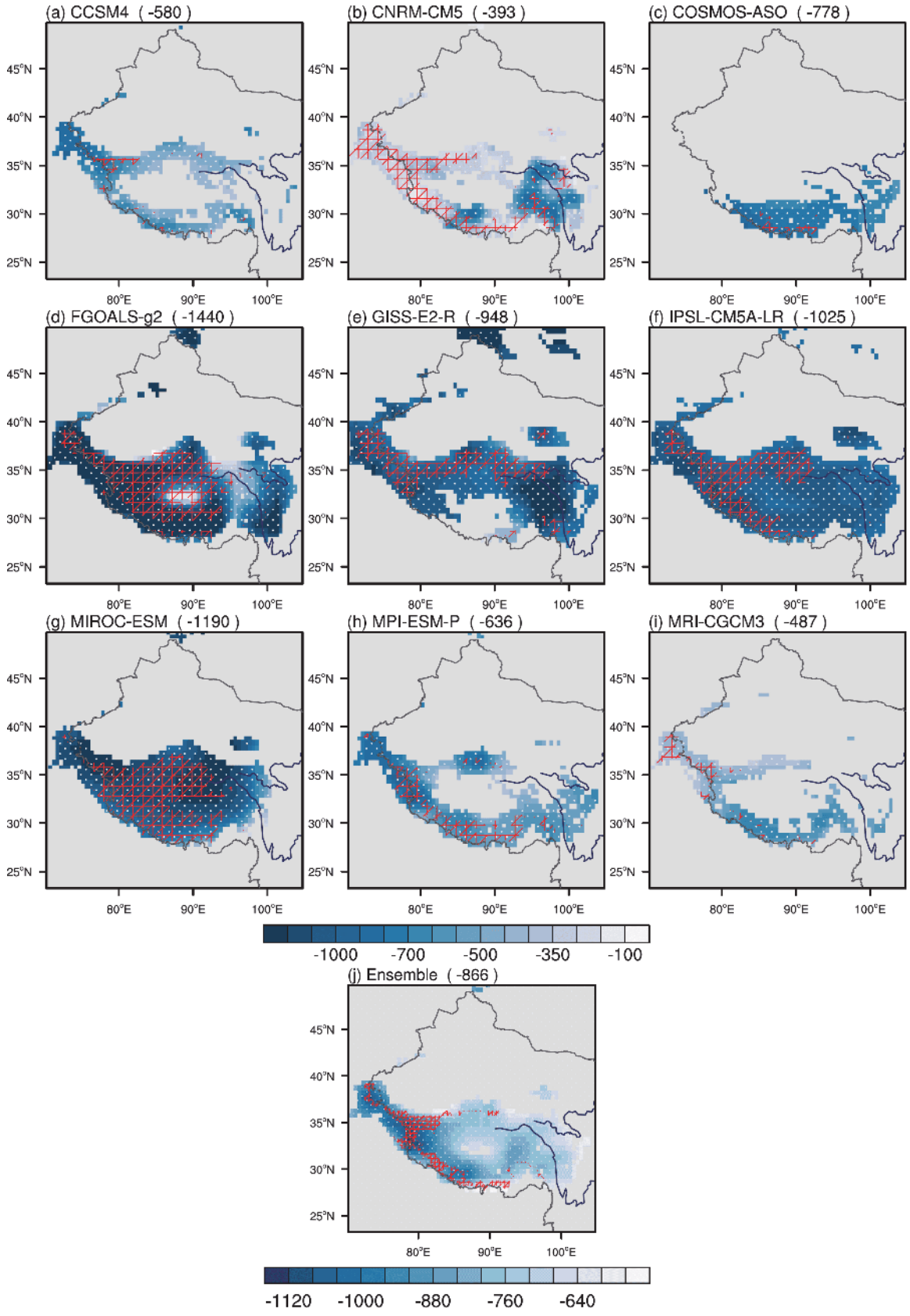

Figure 7 LGM ELA anomalies within the accumulation zones relative to the reference period for individual models and their ensemble mean (m). Gray indicates the LGM non-accumulation zones, and red shading indicates the common areas for both periods. The value in the bracket is the area mean ELA changes over the common areas within China. The dotted areas are significant at the 95% confidence level.

by 244–364 m (Dong et al., 2017), which is qualitatively consistent with the MMM but has smaller amplitudes. Glacier extent mapping and dating indicate that the local maximum glacier advances in the northeastern Tibetan Plateau occurred during the mid-marine isotope stage 3, ahead of the global LGM, and the contemporaneous ELAs were lowered by 786 m (Cui et al., 2018). Such reconstructions generally agree with simulations. Using the technology of luminescence chronology, Chen et al. (2014) examined the glacial landforms in the Parlung Zangbo Valleys of the southeastern Tibetan Plateau and suggested that ELAs in five glaciers declined by an average of 917 m, similar to most of the model results.

4.2 Causes for the LGM ELA changes

The summer temperature and annual precipitation jointly modulate the ELA changes during the LGM. The decrease in the former suppresses glacier ablation and lowers ELAs, and the deficit of the latter decreases glacier supply and accumulation and raises ELAs. For the MMM, the summer temperature and annual precipitation in western China decreased by 4–8°C and 25% during the LGM relative to the reference period, respectively. Based on the previous proxy data, the reconstructed LGM temperature and precipitation in western China are shown in Figure 8 (Shen et al., 1996, 2006; Shi et al., 1997; Ye et al., 1999; Yu et al., 2003; Tang et al., 2004; Herzschuh, 2006; Wan et al., 2008; Herzschuh et al., 2010; Li and Morrill, 2013; Zhao et al., 2013; Wang et al., 2014; Zhao et al., 2015; Li and Liu, 2016). All the records indicate the colder LGM relative to the modern conditions (Figure 8a); the maximum cooling is located at the marginal Tibetan Plateau and the Qilian Mountains; the cooling at the southwestern edges is larger than that at the northeastern edges; these reconstructed characteristics also stand out in simulations. Quantitatively, the LGM Tibetan Plateau is reconstructed to have been colder by 6–9°C (Shen et al., 1996; Shi et al., 1997), which is approximately 1°C lower than the value from simulations. The reconstructed precipitation is complicated and spatially uneven. Most sites display a deficit, but many sites in the Hengduan Mountains, the northwestern Tibetan Plateau, and part of Xinjiang indicate excess precipitation (Figure 8b). The LGM annual precipitation over the Tibetan Plateau is estimated to amount to only 30–70% of that at present (Shi et al., 1997), and hence, the simulated deficit of 25% is relatively smaller.

Relative to the reconstructions from the limited sites, the simulated LGM reductions in temperature and precipitation are underestimated by approximately 1°C and 5–45%, respectively. The former leads to a rise of ELAs by approximately 150 m, while the latter leads to a drop of ELAs by 20–230 m. Such changes in ELAs counteract each other; thus, the simulated ELA reduction is compatible with those from the reconstructions. Liu et al. (1999, 2002) argued that the LGM ELAs declined by 1000–2000 m based on the estimated cooling of 9–11°C, hundreds of meters larger than the values from simulations. One of the reasons for such a discrepancy is that their studies did not fully consider the effect of the precipitation deficit on the ELA rise. Under such remarkable cooling conditions, the deficit in precipitation should be higher than that of the previous estimates of 30–70% (Shi et al., 1997), which should offset the decline in ELAs to a certain degree. In reality, changes in temperature and precipitation are linked with each other at the regional scale. The air temperature decrease could induce less precipitation, and these two factors exert opposite effects on the ELAs with different sensitivities. According to eq. (5), for 100 m rise (decline) in ELAs, the temperature needs to increase (decrease) by 0.65°C or the precipitation to decrease (increase) by 23% (30%). Thus, it can be judged that the simulated reduction in the LGM ELAs by 550–1100 m is mainly caused by the summer cooling of 4–8°C, while the raising effect of less precipitation is limited.

4.3 Causes for the slight ELA reduction in the central Tibetan Plateau

For most models, the reduction in the LGM ELA decreases from the periphery to the center of the Tibetan Plateau. In the four high-resolution models, the ELA reduction is limited within 500 m across most of the plateau (Figure 7a, b, h, and i). According to the paleo-glacier remains, Shi et al. (1997) and Shi (2002b) suggested that the areas with LGM ELA reductions of no more than 500 and 300 m occupy approximately 60% and 40% of the total Tibetan Plateau, respectively; the ELA reduction is less than 200 m in the Tanggula Mountains of the central plateau; and such a small magnitude is relatively rare in the global mountain glaciers, which is thought to be due to the decreased precipitation. Given the contribution from the global sea level fall by more than 100 m (Hanson and Hooke, 2011), the reported ELA reduction in the central plateau might be even less. Based on the CMIP5 simulations, this phenomenon results from a small decrease in temperature but a large deficit in precipitation. In the central Tibetan Plateau, the simulated cooling is only approximately half of the average across the whole plateau, but the percentage reduction in local precipitation is larger than the average. While the cooling induces a decline in ELAs, the lower precipitation exerts an opposite effect. Both effects lead to a slight reduction of ELAs in the central plateau relative to other regions. Note that the climatological precipitation is small in the arid central plateau. The aforementioned small magnitude of reduction actually accounts for a large proportion of precipitation. Therefore, the precipitation deficit considerably modulates the local ELA reduction in the central plateau

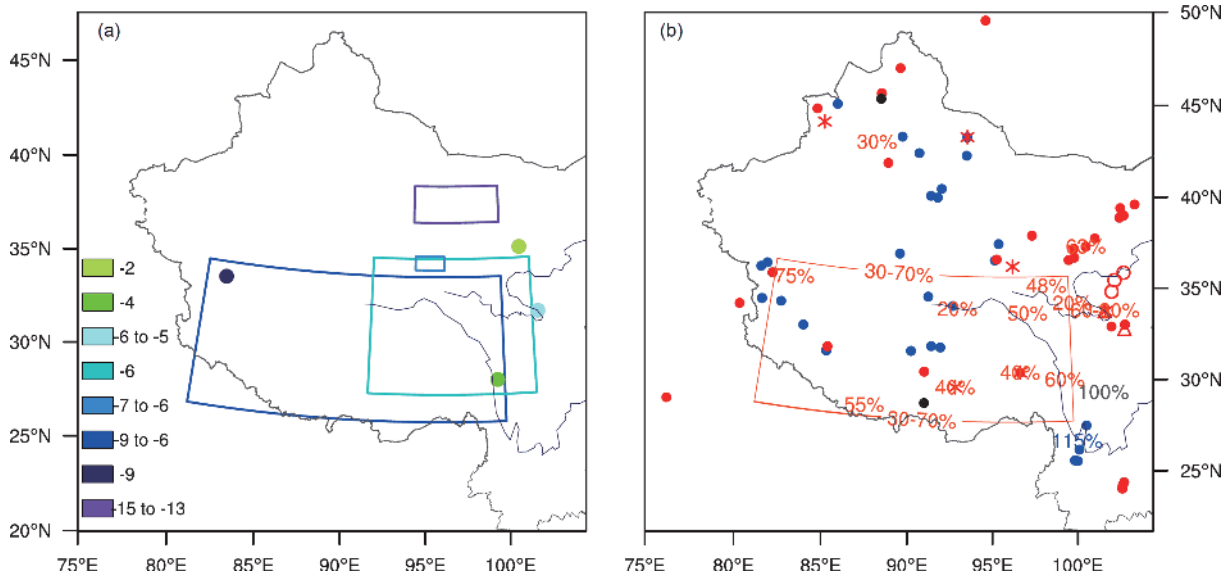

Figure 8 Reconstructions of annul temperature ((a), °C) and precipitation (b) changes in western China during the LGM relative to the present day. In panel (b), markers of dot (•), circle (O), triangle (Δ), and star (*) denote records from lake, loess, pollen, and peat, respectively; blue and red colors denote the LGM precipitation deficit and excess relative to modern conditions, respectively; the numbers in the plot denote the percentage anomaly of precipitation. Maps are drawn using the Lambert projection.

during the LGM. Additionally, the precipitation deficit is mainly associated with the decreased water vapor transport due to the weakening of the South Asian summer monsoon (Jiang and Tian, 2017).

4.4 Comparison to the previous simulations and the uncertainty of simulations

The LGM ELAs on the Tibetan Plateau are lowered by 300–900 m on the basis of the simulations of CCM3 with a horizontal resolution of 2.8°×2.8° (Zhao et al., 2003). However, in our study, the LGM ELAs decline by 550–1100 m and on average by 886 m for the MMM, which are closer to the values estimated by the elevation of cirque glaciers and the rate of accumulation zone area (Shi et al., 1997). Moreover, the CMIP5 models also show better performance regarding the simulation of modern glacier extents and ELA distributions, especially the high-resolution models. The corresponding four models consistently indicate that the accumulation zones expand during the LGM, but these zones are limited to within the marginal mountains and do not reach the central part (Figure 7). In the CCM3 modern and LGM experiments, however, the glaciers are concentrated in the central plateau rather than the high-elevation marginal mountains, which differs from the fact. This outcome might be related to the smooth terrain and the smaller cooling of 2–4°C in the CCM3.

Using a coupled mass-balance and ice-flow model, Xu and Glasser (2015) simulated the LGM glacier extents in the Payuwang Valley of the western Nyainqentanglha Mountains and suggested the local ELAs were approximately 340 m lower than at present. Meanwhile, in the Tashkurgan River Valley of the Karakoram Mountains (Xu et al., 2013) and the Yingpu Valley of the eastern Tibetan Plateau (Xu, 2014), the glacier-climate model simulations indicated that the LGM ELAs declined by 610 and 500 m, respectively. Rupper and Koppes (2010) used the mass and energy balance equation, along with the meteorological variables from the atmospheric general circulation model, to simulate decreases of 1000, 1000, and 500 m in the LGM glacier ELAs over the western, northern, and southern Tibetan Plateau, respectively. In Central Asia, the LGM ELAs of the high-latitude glaciers in the Gobi-Altai and Hangai ranges were respectively 260–590 m and approximately 1000 m lower than the present day and displayed a level of regional differences (Batbaatar et al., 2018). Altogether, except for Central Asia, simulations with various approaches all suggest generally consistent ELA changes in western China during the LGM, although there are some differences in the magnitude.

In our study, the approximation of the precipitation at the ELA by that at the model topographic elevation might have a certain effect on the ELA results, but the amplitude should be small. Generally, the precipitation on the Tibetan Plateau increases with elevation, but it decreases after reaching a certain height. The relationship between precipitation and elevation has been shown to be associated with the water vapor sources. For example, precipitation usually increases with elevation over the East Asian monsoon areas, while the opposite holds for the Indian monsoon areas (Lu et al., 2007). Because there are sparse observation stations in western China, the relationship between precipitation and elevation remains unresolved. According to eq. (5), the ELA rises

(declines) by 100 m when the precipitation decreases (increases) by 23% (30%). The ELAs are overall insensitive to precipitation variations. In other words, precipitation variation within a certain range has little influence on the ELAs. Additionally, the ELA calculated from the empirical relationship between temperature and precipitation refers to the lowest elevation climatically suited for glacier formation, and the accumulation zones are the ranges climatically suited for net glacier accumulation. The actual formation of glaciers within a certain area is also closely related to the local topography, the grade and direction of slope, and even the wind field (Figure 1). Though some models simulate continuous accumulation zones on the Tibetan Plateau, the actual distribution of glaciers is not necessarily continuous but is most likely scattered across mountains.

5. Conclusions

The nine CMIP5 models reasonably simulate the temperatures, precipitation, ELAs, and glaciers in western China during the reference period. Our analysis of the LGM simulations yields the following conclusions.

(1) Relative to the reference period, the LGM summer temperatures over the Tibetan Plateau decrease by 4–8°C. The cooling is the smallest in the central part and amplifies toward the edges, especially for the southern and western margins. The percentage of annual precipitation deficit tends to increase from the southern and western margins to the northeast and averages 25% for the whole Tibetan Plateau.

(2) The summer cooling and annual precipitation deficit lead to the fall and rise of the ELA during the LGM, respectively, but the former contribution is predominant. The ELAs within the Tibetan Plateau accumulation zones decrease by 550–1100 m and by an average of 866 m. The maximum reduction is located in the southern and western marginal mountains, coinciding with the maximum cooling centers, while the minimum decrease appears in the arid central plateau where the reduction is partly counteracted by the ELA rise due to the considerable deficit in precipitation. Compared to the reference period, The LGM ELAs decrease by 500–600 m in the Altai and Qilian Mountains within China and by less than 650 m in the Tian Shan Mountains. Generally, the simulated ELA reductions and their spatial patterns are compatible with the records from paleo-glaciers.

(3) The LGM accumulation zones in western China expand to 2–5 times the modern range. The four high-resolution models suggest that the accumulation zones expand from the marginal to the central Tibetan Plateau but still do not cover the entire plateau.

Acknowledgements *We sincerely thank the two anonymous reviewers for their insightful comments and suggestions to improve this manuscript. We also acknowledge the climate modelling groups (listed in Table 1) for producing and sharing their model outputs. This work was supported by the Strategic Priority Research Program of the Chinese Academy of Sciences (Grant No. XDA20070103) and the National Natural Science Foundation of China (Grant Nos. 41625018 & 41421004).*

References

Batbaatar J, Gillespie A R, Fink D, Matmon A, Fujioka T. 2018. Asynchronous glaciations in arid continental climate. Quat Sci Rev, 182: 1–19

Bravo C, Rojas M, Anderson B M, Mackintosh A N, Sagredo E, Moreno P I. 2015. Modelled glacier equilibrium line altitudes during the mid-Holocene in the southern mid-latitudes. Clim Past, 11: 1575–1586

Chen R, Zhou S, Lai Z, Ou X, Chen R, Deng Y. 2014. Luminescence chronology of Late Quaternary moraines and Last Glacial Maximum equilibrium-line altitude reconstruction from Parlung Zangbo Valley, south-eastern Tibetan Plateau. J Quat Sci, 29: 597–604

Clark P U, Dyke A S, Shakun J D, Carlson A E, Clark J, Wohlfarth B, Mitrovica J X, Hostetler S W, McCabe A M. 2009. The last glacial maximum. Science, 325: 710–714

Cui H, Wang J, Yu B, Hu Z, Yao P, Harbor J M. 2018. Marine Isotope Stage 3 paleotemperature inferred from reconstructing the Die Shan ice cap, northeastern Tibetan Plateau. Quat Res, 89: 494–504

Dong G, Xu X, Zhou W, Fu Y, Zhang L, Li M. 2017. Cosmogenic ^{10}Be surface exposure dating and glacier reconstruction for the Last Glacial Maximum in the Quemuqu Valley, western Nyainqentanglha Mountains, south Tibet. J Quat Sci, 32: 639–652

Duan K, Yao T, Shi P, Guo X. 2017. Simulation and prediction of equilibrium line altitude of glaciers in the eastern Tibetan Plateau (in Chinese). Sci Sin Terrae, 47: 104–113

Hanson B, Hooke R L B. 2011. Effect of sea-level lowering on ELA depression during the LGM. Quat Res, 75: 406–410

Hebenstreit R. 2006. Present and former equilibrium line altitudes in the Taiwanese high mountain range. Quat Int, 147: 70–75

Herzschuh U. 2006. Palaeo-moisture evolution in monsoonal Central Asia during the last 50000 years. Quat Sci Rev, 25: 163–178

Herzschuh U, Birks H J B, Mischke S, Zhang C, Böhner J. 2010. A modern pollen-climate calibration set based on lake sediments from the Tibetan Plateau and its application to a Late Quaternary pollen record from the Qilian Mountains. J Biogeogr, 37: 752–766

Heyman J. 2014. Paleoglaciation of the Tibetan Plateau and surrounding mountains based on exposure ages and ELA depression estimates. Quat Sci Rev, 91: 30–41

Hu G, Yi C, Zhang J, Dong G, Liu J, Xu X, Jiang T. 2017. Extensive glacial advances during the last glacial maximum near the eastern Himalayan syntaxis. Quat Int, 443: 1–12

Hu Q, Jiang D, Fan G. 2014. Evaluation of CMIP5 models over the Qinghai-Tibetan Plateau (in Chinese). Chin J Atmos Sci, 38: 924–938

Jiang D, Liang X. 2008. Attribution of East Asian climate at the last glacial maximum (in Chinese). Quat Sci, 28: 491–501

Jiang D, Tian Z, Lang X, Kageyama M, Ramstein G. 2015. The concept of global monsoon applied to the last glacial maximum: A multi-model analysis. Quat Sci Rev, 126: 126–139

Jiang D, Tian Z. 2017. Last glacial maximum and mid-Holocene water vapor transport over East Asia: A modeling study (in Chinese). Quat Sci, 37: 999–1008

Kuhle M. 1995. Glacial isostatic uplift of Tibet as a consequence of a former ice sheet. GeoJournal, 37: 431–449

Li Y, Liu Y. 2016. The response of lake records to the circulation system and climate zones in China since the last glacial maximum (in Chinese). Acta Geogr Sin, 71: 1898–1910

Li Y, Morrill C. 2013. Lake levels in Asia at the last glacial maximum as indicators of hydrologic sensitivity to greenhouse gas concentrations. Quat Sci Rev, 60: 1–12

Lie Ø, Dahl S O, Nesje A. 2003. A theoretical approach to glacier equi-

librium-line altitudes using meteorological data and glacier mass-balance records from southern Norway. Holocene, 13: 365–372
Liu T, Zhang X, Xiong S, Qin X. 1999. Qinghai-Xizang Plateau glacial environment and global cooling (in Chinese). Quat Sci, 19: 385–396
Liu T, Zhang X, Xiong S, Qin X, Yang X. 2002. Glacial environments on the Tibetan Plateau and global cooling. Quat Int, 97-98: 133–139
Liu Y, Jiang D. 2016. Last glacial maximum permafrost in China from CMIP5 simulations. Palaeogeogr Palaeoclimatol Palaeoecol, 447: 12–21
Lu C, Wang L, Xie G, Leng Y. 2007. Altitude effect of precipitation and spatial distribution of Qinghai-Tibetan Plateau (in Chinese). J Mt Sci, 25: 655–663
Ono Y, Shulmeister J, Lehmkuhl F, Asahi K, Aoki T. 2004. Timings and causes of glacial advances across the PEP-II transect (East-Asia to Antarctica) during the last glaciation cycle. Quat Int, 118-119: 55–68
Rupper S, Koppes M. 2010. Spatial patterns in Central Asian climate and equilibrium line altitudes. IOP Conf Ser-Earth Environ Sci, 9: 012009
Rupper S, Roe G. 2008. Glacier changes and regional climate: A mass and energy balance approach. J Clim, 21: 5384–5401
Saito K, Sueyoshi T, Marchenko S, Romanovsky V, Otto-Bliesner B, Walsh J, Bigelow N, Hendricks A, Yoshikawa K. 2013. LGM permafrost distribution: How well can the latest PMIP multi-model ensembles perform reconstruction? Clim Past, 9: 1697–1714
Shen C, Liu K, Tang L, Overpeck J T. 2006. Quantitative relationships between modern pollen rain and climate in the Tibetan Plateau. Rev Palaeobot Palynol, 140: 61–77
Shen C, Tang L, Wang S. 1996. Vegetation and climate during the last 250000 years in Zoigê region (in Chinese). Acta Micropal Sin, 13: 373–385
Shi Y. 2002a. Characteristics of Late Quaternary monsoonal glaciation on the Tibetan Plateau and in East Asia. Quat Int, 97-98: 79–91
Shi Y. 2002b. Discussion on temperature lowering values and equilibrium lines altitude in the Qinghai-Xizang Plateau during the last glacial maximum and their simulated results (in Chinese). Quat Sci, 22: 312–322
Shi Y, Cui Z, Li J. 1989. The Problems of Quaternary Glacier and Environment in East China (in Chinese). Beijing: Science Press. 462
Shi Y, Cui Z, Su Z. 2006. The Quaternary Glaciations and Environmental Variations in China (in Chinese). Shijiazhuang: Hebei Science and Technology Publishing House. 618
Shi Y, Huang M, Yao T, Deng Y. 2000. Glaciers and Their Environments in China—The present, past and future (in Chinese). Beijing: Science Press. 410
Shi Y, Zheng B, Yao T. 1997. Glaciers and environments during the last glacial maximum (LGM) on the Tibetan Plateau (in Chinese). J Glaciol Geocryol, 19: 97–113
Su Z, Zhao J, Zheng B. 2014. Distribution and features of the glaciers' ELAs and the decrease of ELAs during the last glaciation in China (in Chinese). J Glaciol Geocryol, 36: 9–19
Tang L, Shen C, Liu K, Yu S, Li C. 2004. Climatic changes in the southwestern Qinghai-Tibetan Plateau since the last glacial maximum – pollen records from southwestern Tibet (in Chinese). Sci China Ser D-Earth Sci, 34: 436–442
Taylor K E, Stouffer R J, Meehl G A. 2012. An overview of CMIP5 and the experiment design. Bull Amer Meteorol Soc, 93: 485–498
Tian Z P, Jiang D B. 2015. Mid-Holocene and last glacial maximum changes in monsoon area and precipitation over China. Chin Sci Bull, 60: 400–410
Tian Z, Jiang D. 2016. Revisiting last glacial maximum climate over China and East Asian monsoon using PMIP3 simulations. Palaeogeogr Palaeoclimatol Palaeoecol, 453: 115–126
Ueda H, Kuroki H, Ohba M, Kamae Y. 2011. Seasonally asymmetric transition of the Asian monsoon in response to ice age boundary conditions. Clim Dyn, 37: 2167–2179
Wan H, Tang L, Zhang H, Li C, Pang Y. 2008. Pollen record reflects climate changes in eastern Qaidam Basin during 36–18 ka B.P. (in Chinese). Quat Sci, 28: 112–121
Wang S, Wen X. 2011. Last glacial maximum (in Chinese). Adv Clim Change Res, 7: 381–382
Wang Y, Herzschuh U, Shumilovskikh L S, Mischke S, Birks H J B, Wischnewski J, Böhner J, Schlütz F, Lehmkuhl F, Diekmann B, Wünnemann B, Zhang C. 2014. Quantitative reconstruction of precipitation changes on the NE Tibetan Plateau since the Last Glacial Maximum-extending the concept of pollen source area to pollen-based climate reconstructions from large lakes. Clim Past, 10: 21–39
Wu J, Gao X. 2013. A gridded daily observation dataset over China region and comparison with the other datasets (in Chinese). Chin J Geophys, 56: 1102–1111
Xu X. 2014. Climates during Late Quaternary glacier advances: Glacier-climate modeling in the Yingpu Valley, eastern Tibetan Plateau. Quat Sci Rev, 101: 18–27
Xu X, Glasser N F. 2015. Glacier sensitivity to equilibrium line altitude and reconstruction for the last glacial cycle: Glacier modeling in the Payuwang Valley, western Nyaiqentanggulha Shan, Tibetan Plateau. Palaeogeogr Palaeoclimatol Palaeoecol, 440: 614–620
Xu X, Hu G, Qiao B. 2013. Last glacial maximum climate based on cosmogenic ^{10}Be exposure ages and glacier modeling for the head of Tashkurgan Valley, northwest Tibetan Plateau. Quat Sci Rev, 80: 91–101
Yan M, Wang B, Liu J. 2016. Global monsoon change during the last glacial maximum: A multi-model study. Clim Dyn, 47: 359–374
Ye B S, Ding Y J, Shi Y F, Zheng B X. 1999. A study of the climate and the environment during the last glacial maximum in western China. In: Tranter M, Armstrong R, Brun E, eds. Interactions Between the Cryosphere, Climate and Greenhouse Gases. Bellingham: IAHS-AISH Publication. 217–225
Yu G, Xue B, Liu J, Chen X. 2003. LGM lake records from China and an analysis of climate dynamics using a modelling approach. Glob Planet Change, 38: 223–256
Zhang W, Cui Z, Yan L. 2009. Present and late Pleistocene equilibrium line altitudes in Changbai Mountains, Northeast China. J Geogr Sci, 19: 373–383
Zhao K, Li X, Dodson J, Zhou X, Atahan P. 2013. Climate instability during the last deglaciation in Central Asia, reconstructed by pollen data from Yili Valley, NW China. Rev Palaeobot Palynol, 189: 8–17
Zhao P, Chen L, Zhou X, Gong Y, Han Y. 2003. Modeling the East Asian climate during the last glacial maximum. Sci China Ser D-Earth Sci, 46: 1060–1068
Zhao Y, An C B, Mao L, Zhao J, Tang L, Zhou A, Li H, Dong W, Duan F, Chen F. 2015. Vegetation and climate history in arid western China during MIS2: New insights from pollen and grain-size data of the Balikun Lake, eastern Tien Shan. Quat Sci Rev, 126: 112–125

(Responsible editor: Huayu LU)